Quantum gate operations using midinfrared binary shaped pulses on the rovibrational states of carbon monoxide

Ryan R. Zaari and Alex Brown[a)]
Department of Chemistry, University of Alberta, Edmonton, Alberta T6G 2G2, Canada

(Received 13 October 2009; accepted 18 December 2009; published online 6 January 2010)

Frequency domain shaped binary laser pulses were optimized to perform 2 qubit quantum gate operations in $^{12}C^{16}O$. The qubit rovibrational state representation was chosen so that all gate operations consisted of one-photon transitions. The amplitude and phase varied binary pulses were determined using a genetic algorithm optimization routine. Binary pulses have two possible amplitudes, 0 or 1, and two phases, 0 or π, for each frequency component of the pulse. Binary pulses are the simplest to shape experimentally and provide a minimum fidelity limit for amplitude and phase shaped pulses. With the current choice of qubit representation and using optimized binary pulses, fidelities of 0.80 and as high as 0.97 were achieved for the controlled-NOT and alternative controlled-NOT quantum gates. This indicates that with a judicious choice of qubits, most of the required control can be obtained with a binary pulse. Limited control was observed for 2 qubit NOT and Hadamard gates due to the need to control multiple excitations. The current choice of qubit representation produces pulses with decreased energies and superior fidelities when compared with rovibrational qubit representations consisting of two-photon transitions. The choice of input pulse energy is important and applying pulses of increased energy does not necessarily lead to a better fidelity. © *2010 American Institute of Physics*. [doi:10.1063/1.3290957]

I. INTRODUCTION

Laser control of molecules has seen its greatest development in the past two decades due to advancements in experimental laser sources and our theoretical understanding of the underlying principles of control.[1–5] These developments have opened the door to femtosecond and emerging attosecond science. The use of lasers allows for more specific control of molecules, from the individual nuclei in reaction dynamics[5] to the individual electrons of a molecule.[6–8] It has been proposed that laser control of molecular states could be used as a construction for quantum logic gates within quantum computing[9] and numerous studies have followed this suggestion, see, for example, Refs. 10–15. A fully functioning quantum computer would allow for many applications and uses, but solving quantum mechanical problems exactly would be one of the most important. The full capability of outperforming a classical computer resides in a quantum computer's ability to create superposition states, something that a classical computer cannot do.

Currently molecular quantum computing is seeing studies from all aspects such as controlling nuclear states using nuclear magnetic resonance,[16,17] electronic states in ion traps,[18,19] and the control of rovibrational states with shaped laser pulses,[20] the last of which is relevant here. Within rovibrational control, a laser field is used to manipulate the rovibrational states of a molecule in order to create a series of quantum logic gate operations from which quantum algorithms can be implemented. As there are classical logic operations in traditional Boolean algebra, there is also a set of analogous quantum logic operations. Each laser field is designed to behave as a certain quantum logic gate and would act on chosen rovibrational states representing the qubits (quantum bits), inevitably executing a quantum algorithm. Currently there are two main theoretical methods to determine the optimal laser fields (not limited to quantum logic gate operations): optimal control theory (OCT)[3,21] and the genetic algorithm (GA),[22] along with some other less common methods such as simulated annealing[23] and ant colony optimization.[24] OCT often relies on an iterative method which maximizes a functional, composed in part by a time dependent laser field term. The most desirable laser field is one which produces the greatest value for the functional. Since, in general, there are no explicit restrictions on the possible laser fields produced by the OCT method, they can contain frequencies which are not attainable by current experimental pulse shaping techniques. OCT has been used to study quantum gate operations, using the vibrational states of OH (Ref. 10) or the rovibrational states of CO.[11] In the case of using OCT on larger systems such as acetylene[12] and $MnBr(CO)_5$,[13] the vibrational modes were chosen to represent the qubits, while also using reduced dimensional models of the system. The GA has been used to optimize quantum gate operations using the rovibrational states of thiophosgene ($SCCl_2$) (Ref. 14) and also CO.[15] The GA optimization, which is implemented in this study, selects the desired properties of the laser field in the frequency domain and thus mimics the experimental laser pulse shaping procedures using a feedback loop. The GA searches for frequency dependent amplitude and phase components that construct laser pulses producing the greatest fidelity for the chosen quantum

[a)]Electronic mail: alex.brown@ualberta.ca.

logic gate. For rovibrational state control, the range of frequencies available is in the midinfrared (mid-IR) regime.

There are few aspects of molecular quantum computing using shaped mid-IR laser pulses that have been investigated to indicate strengths and weaknesses of such a procedure. There are many adjustable parameters of the pulse shaper that can affect the resulting quantum gate fidelity. These include the frequency resolution of the shaper, the central frequency, the bandwidth, the input laser pulse energy, and the range of amplitude and phase values. Alternatively, there are also intrinsic molecular properties that can dictate resulting quantum gate fidelities, such as the rovibrational state energies, transition dipole moments, available selection rules, and the choice of qubit rovibrational state representation. A poor choice of the rovibrational states to represent the qubits may result in ineffective population transfer and thus lower the fidelity of the gate operation. In this paper, we investigate the effects of a restricted range of amplitude and phase values (binary pulse), as well as an alternative choice of rovibrational states to represent the qubits, on quantum gate fidelities. These results are compared with previous work on $^{12}C^{16}O$ by Tsubouchi and Momose.[15] In their study, they chose qubit representations of the rovibrational states that resulted in some two-photon quantum gate operations. As will be shown here, all gates can be reduced to one-photon transitions through judicious choice of the qubit states. The number of possible amplitude and phase values within a given range is another important factor. More values within the range means greater variation in the attributes of the resulting pulsed laser field. However, this puts a large burden on the GA optimization's ability to search efficiently through these values for the greatest fidelity. The simplest shaped laser pulse consists of a choice of two amplitude (0 or 1) and two phase values (0 or π) for each frequency component and this is denoted as a binary laser pulse. The GA optimization can then efficiently find the greatest fidelity within this reduced, but still extremely large, search space. Moreover, all other possible shaped laser pulses which contain more than two values of amplitude and phase within this range will have search spaces that also contain the binary laser pulse as a possible solution. Thus, the binary laser pulse sets a lower bound on the possible fidelities that can be obtained with the GA optimization method for a specific quantum logic gate. In comparison, Tsubouchi and Momose[15] chose a range of 64 choices each for the amplitude and phase, thus producing an extremely large search space. In summary, binary laser pulses were optimized in the frequency domain using a GA procedure to carry out common quantum gate operations. Specific rovibrational states of $^{12}C^{16}O$ were chosen to represent the qubits such that single photon transitions would result.

II. THEORY

The model system chosen was the rovibrational states of carbon monoxide ($^{12}C^{16}O$) in its ground electronic state. Select rovibrational states of CO are chosen to represent the qubits and the quantum gate operations are carried out by shaped binary pulses. The projection quantum number J_z along the total angular momentum J is zero. The rovibrational states are represented with the vibrational quantum number ν and the rotational quantum number J in the form (νJ). The CO model consists of seven vibrational states ranging from $\nu=0$ to 6, each containing nine rotational states ranging from $J=0$ to 8. These energies were obtained by Mantz *et al.*[25] using a linear fit of the molecular constants to a power series of both rotational and vibrational term values. The accessible rovibrational states are $\Delta\nu=\pm 1$ and $\Delta J=\pm 1$ due to selection rules and the utilization of mid-IR pulses. It is important to point out that previous work by Shioya *et al.*[11] also on CO, but using iterative OCT, produced laser pulses that contained both microwave and IR frequencies. This allowed them to have independent control of rotational or vibrational states, which is not permitted here. Binary (two amplitude and two phase) laser field pulses with frequency domain optimization are chosen. Tsubouchi and Momose[15] chose to carry out similar calculations on CO also with GA optimization but using much larger 64 amplitude and 64 phase varied laser pulses and a different choice of states for the qubits. A comparison between our results and those of Tsubouchi and Momose[15] is made in the results, see Sec. III A.

A. Quantum mechanical system

In the present work, the objective is to determine a laser field which directs the system from an initial state to a final target state. Moreover, in this study, the laser pulses are designed to perform unitary quantum logic gate operations on the rovibrational state wave functions of CO, but in general this can extend beyond simple population control. The time-dependent Schrödinger equation (TDSE) with the Hamiltonian $H(r,t)$, describing the laser pulse/molecular dipole interaction, is

$$i\hbar\frac{d\Psi(r,t)}{dt}=H(r,t)\Psi(r,t)=[H_0(r)-\epsilon(t)\mu(r)]\Psi(r,t), \tag{1}$$

where $H_0(r)$ is the time-independent rovibrational Hamiltonian, $\epsilon(t)$ is the electric field of the laser pulse, and $\mu(r)$ is the molecular dipole moment.

The molecular wave function $\Psi(r,t)$ is represented in the familiar linear time-dependent form as

$$\Psi(r,t)=\sum_{\nu J}c_{\nu J}(t)\psi_{\nu J}(r), \tag{2}$$

where we have a linear combination of time-dependent rovibrational coefficients $c_{\nu J}(t)$ and stationary states $\psi_{\nu J}(r)$. Rewriting the TDSE in terms of the time-dependent coefficients $c_{\nu J}(t)$ in matrix notation results in an equation of the form

$$\dot{\underline{c}}(t)=-\frac{i}{\hbar}[\underline{\underline{E}}-\epsilon(t)\underline{\underline{\mu}}]\underline{c}(t). \tag{3}$$

The time-dependent coefficients are now contained in a rovibrational state vector $\underline{c}(t)$ and the Hamiltonian consists of a square energy matrix $(\underline{\underline{E}})$ along with a square transition dipole matrix $(\underline{\underline{\mu}})$ with matrix elements based upon the allowed transitions of ν and J. The energies were obtained from the

results of work by Mantz *et al.*[25] who used linear fits of the molecular constants. The transition dipole moments were obtained from the results of work by Goorvitch and Chackerian[26] who used polynomial fits relative to the angular momentum quantum number. The goal is to find the optimal electric field (laser pulse) $\epsilon(t)$ to cause the desired quantum gate operation. For a given electric field, the equation is integrated using the fourth-order Runge–Kutta method. The time step used in the integration is the ratio between the number of time points (2^{20}) and the total pulse duration (6.67 ps), which in this study results in $dt=0.0064$ fs. This value is much smaller than the oscillation period.

B. Molecular qubit basis

A "qubit" is the shorthand name given to a "quantum bit," which is analogous to the bit in classical computing. It is a representation of the state of the system and thus is written in the general form $|q_1\ q_2\rangle$, where q_1 and q_2 are denoted as the first and second qubits, respectively. The qubits can be represented in two different ways. The first case entails that each qubit is represented by a separate two-level or quasi-two-level system, and then these n qubits are appropriately coupled.[16–19] Alternatively, and the choice used herein, n qubits can be represented by $N=2^n$ combinations of N molecular states.[14,20,27] We have chosen four rovibrational states of CO to encode the 2 qubit basis using the latter representation. The proper choice of rovibrational states to represent the qubits is important when attempting to control quantum gates with a laser pulse. In the scenario where there is independent control of vibrational and rotational state transitions,[11] an obvious choice has been the rovibrational states $(\nu J)=(00)$, (01), (10), and (11) to represent the qubit states $|00\rangle$, $|01\rangle$, $|10\rangle$, and $|11\rangle$ qubits, respectively. The required excitations will involve one-photon transitions, but will require frequencies both in the mid-IR and microwave regions. In the case studied here, where there must be simultaneous vibrational and rotational state transitions, due to the absorption of mid-IR radiation, the above choice of qubits would result in forbidden transitions according to the allowed transitions. Previous work by Tsubouchi and Momose[15] alluded to the idea that quantum gate operations which consist of two-photon transitions seem to be poorly controlled with a shaped mid-IR laser pulse. Therefore, it would be ideal to have quantum gate operations which consist of one-photon transitions. The qubit basis chosen in this work is shown in Fig. 1. For the controlled-NOT (CNOT), alternative controlled-NOT (ACNOT), NOT, and Hadamard (Had) quantum gates, the transitions encountered all remain single photon and as a consequence the rovibrational state arrangement is cyclic.

C. Quantum gates

A set of universal quantum gates is desirable because any quantum operation, in principle, can then be represented by a combination of this finite set. In the present study, the NOT, Had, CNOT, and ACNOT gates are studied, as shown in Table I. The Had gate, CNOT gate, and the phase gate (not shown) comprise one such set of universal quantum gates.

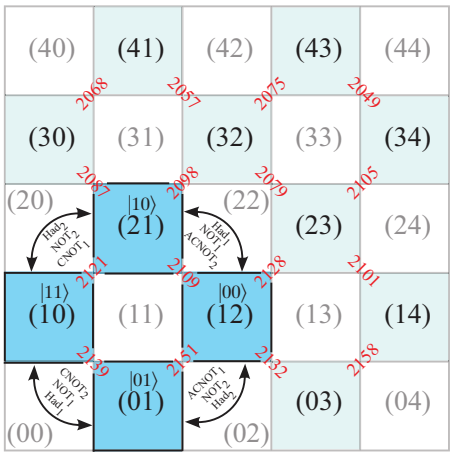

FIG. 1. Illustration of the low-lying rovibrational states of $^{12}C^{16}O$ labeled as (νJ). The accessible states are highlighted (shaded light blue boxes). The chosen qubit representations (shaded dark blue boxes) are labeled as $|q_1q_2\rangle$. Available transitions are governed by the following simultaneous vibrational and rotational transitions, $\Delta\nu=\pm1$ and $\Delta J=\pm1$, which are illustrated by states connected along a diagonal. Some rovibrational states are inaccessible (white boxes). Excitation frequencies (red text) are in cm^{-1} and lie between the accessible rovibrational states. The qubits ($|00\rangle$,$|01\rangle$,$|10\rangle$,$|11\rangle$) that undergo a state change (black arrows) during an applied quantum gate operation, according to Table I, are labeled by the corresponding gate. Notice that the NOT and Had gates require simultaneous control of two transitions.

The NOT and Had quantum gates are labeled such that the number following the gate name refers to whether the gate operates on the first or second qubit. In the case of the CNOT and ACNOT gates, the labeling refers to whether the control qubit is the first or second qubit.

If the vibrational and rotational states could be controlled independently, then the NOT and Had gates would be considered 1 qubit operations. This means that the 2 qubit state can be written as $|q_1\ q_2\rangle=|q_1\rangle|q_2\rangle$, where qubit1 encodes the vibrational states and qubit2 encodes the rotational states. The result is that either qubit1 or qubit2 will be independent upon the operation and the gate only needs to act on one of the qubits. Hence, it is called a 1 qubit operation. As pointed out previously, the laser pulses used in the current study are shaped using frequencies in the mid-IR to induce simultaneous vibrational and rotational transitions. However, this qubit representation cannot treat qubit1 and qubit2 separately and so both the NOT and Had quantum gate operations resemble 2 qubit operations.

The efficiency of a quantum gate operation is determined by the gate fidelity[28,29]

$$F=\frac{1}{N^2}\left|\sum_{k=1}^{N}\langle\Psi_k(T)|\Phi_k\rangle\right|^2, \tag{4}$$

where $\Psi_k(T)$ is the resulting wave function after the laser pulse of duration T has been applied and Φ_k is the target wave function. The wave functions are summed over the number of transitions N and then divided by a normalization factor N^2 to ensure the fidelity ranges between 0 and 1. A fidelity of 1 implies a complete population transfer within the quantum gate operation, as well as the target states being globally phase aligned, as described by

TABLE I. Quantum gate operations which are implemented by an optimized laser pulse. NOT/Had: the number following the gate name refers to which qubit the gate operates on. CNOT/ACNOT: the number following the gate name refers to which qubit is the control qubit.

NOT_1:	$\|00\rangle \leftrightarrow \|10\rangle$	NOT_2:	$\|00\rangle \leftrightarrow \|01\rangle$
	$\|01\rangle \leftrightarrow \|11\rangle$		$\|10\rangle \leftrightarrow \|11\rangle$
Had_1:	$\|00\rangle \leftrightarrow \frac{1}{\sqrt{2}}(\|00\rangle + \|10\rangle)$	Had_2:	$\|00\rangle \leftrightarrow \frac{1}{\sqrt{2}}(\|00\rangle + \|01\rangle)$
	$\|01\rangle \leftrightarrow \frac{1}{\sqrt{2}}(\|01\rangle + \|11\rangle)$		$\|01\rangle \leftrightarrow \frac{1}{\sqrt{2}}(\|00\rangle - \|01\rangle)$
	$\|10\rangle \leftrightarrow \frac{1}{\sqrt{2}}(\|00\rangle - \|10\rangle)$		$\|10\rangle \leftrightarrow \frac{1}{\sqrt{2}}(\|10\rangle + \|11\rangle)$
	$\|11\rangle \leftrightarrow \frac{1}{\sqrt{2}}(\|01\rangle - \|11\rangle)$		$\|11\rangle \leftrightarrow \frac{1}{\sqrt{2}}(\|10\rangle - \|11\rangle)$
$CNOT_1$:	$\|00\rangle \rightarrow \|00\rangle$	$CNOT_2$:	$\|00\rangle \rightarrow \|00\rangle$
	$\|01\rangle \rightarrow \|01\rangle$		$\|10\rangle \rightarrow \|10\rangle$
	$\|10\rangle \leftrightarrow \|11\rangle$		$\|01\rangle \leftrightarrow \|11\rangle$
$ACNOT_1$:	$\|10\rangle \rightarrow \|10\rangle$	$ACNOT_2$:	$\|01\rangle \rightarrow \|01\rangle$
	$\|11\rangle \rightarrow \|11\rangle$		$\|11\rangle \rightarrow \|11\rangle$
	$\|00\rangle \leftrightarrow \|01\rangle$		$\|00\rangle \leftrightarrow \|10\rangle$

$$|\Psi_{00}\rangle + |\Psi_{01}\rangle + |\Psi_{10}\rangle + |\Psi_{11}\rangle \rightarrow (|\Psi_{00}\rangle' + |\Psi_{01}\rangle' + |\Psi_{10}\rangle' + |\Psi_{11}\rangle')e^{i\phi}, \tag{5}$$

where $|\Psi\rangle$ is the state of the qubit initially, $|\Psi\rangle'$ is the state of the qubit after operation by a quantum gate, and $e^{i\phi}$ is the acquired global phase.

The fidelity function enforces the global phase correction, which is an important feature in order to apply quantum gates sequentially, as described by Tesch and de Vivie-Riedle.[29] If one uses an iterative OCT algorithm to determine the quantum gates, additional transitions to those shown in Table I must be optimized to ensure global phase alignment. However, for the GA procedure (or any other stochastic algorithm), the optimization of these additional transitions is not needed as the fidelity, Eq. (4), is used explicitly to judge the fitness of a particular laser pulse during the optimization.

The average final state population, which does not incorporate phase alignment, is given by

$$\bar{P} = \frac{1}{N}\sum_{k=1}^{N} |\langle \Psi_k(T)|\Phi_k\rangle|^2. \tag{6}$$

Although not used within the optimization algorithm as a means to judge the fitness of the laser pulses, Eq. (6) does give an indication of the ability of the laser pulse to transfer population without global phase alignment.

D. Laser pulse optimization

The laser pulses used to carry out the individual quantum gate operations are constructed in the frequency domain. The shaped laser pulse, written in terms of the frequency components ν_j, is modeled by[15]

$$\epsilon(\nu_j) = \epsilon_0\sqrt{A(\nu_j)}\,\exp\left[-2\ln 2\left(\frac{\nu_j - \nu_0}{\Delta\nu}\right)^2\right]\exp[i\phi(\nu_j)], \tag{7}$$

where ϵ_0 is the peak field strength, ν_0 is the central frequency, and ν_j represents the discrete frequencies at which the field is shaped. The amplitude and phase range from $0 \le A(\nu_j) \le 1$ and $0 \le \phi(\nu_j) \le 2\pi$, respectively. The transform limited (TL) pulse, which is the input pulse for experimental pulse shaping, defines the pulse structure which is to be shaped. The TL pulse is defined by $A(\nu_j)=1$ and $\phi(\nu_j)=0$ in Eq. (7). The amplitude and phase components can be adjusted independently, producing a shaped pulse with defined amplitude and phase features. This shaped pulse is bound by the structure of the TL pulse such as its bandwidth, amplitude, and by the physical pulse shaper frequency discretization. The TL pulse used has a Gaussian profile with a full width at half-maximum (FWHM) pulse width of $\Delta\nu = 100\ \text{cm}^{-1}$. The central frequency ν_0 is dependent upon the quantum gate operation being optimized and is chosen to be the average resonant frequency of the transition involved for the specific qubit change. The bandwidth of frequencies ranges from $\pm 250\ \text{cm}^{-1}$ of the central frequency. The pulse shaper was arbitrarily chosen to contain 51 discrete ampli-

TABLE II. Optimal fidelities F for the quantum logic gates studied using the specified qubit representation (Fig. 1) of the rovibrational states of $^{12}C^{16}O$. The associated central frequency, TL and optimized pulse energies, and peak intensity and average populations are also shown (NR—not reported).

Quantum gate	Central frequency, ν_0 (cm^{-1})	Pulse energy (TL-pulse energy) (μJ)	Peak intensity (TW/cm^2)	Fidelity, F/average population, $\bar{P}$
$CNOT_1$	2121	2.20 (5)	0.0466	0.8113/0.9814
$CNOT_2$	2139	4.55 (10)	0.0896	0.7962/0.8241
$ACNOT_1$	2151	4.07 (10)	0.0901	0.9729/0.9904
$ACNOT_2$	2109	0.77 (5)	0.033	0.8416/0.9302
Had_1	2124	13.21 (30)	0.229	0.6172/0.6294
Had_2	2136	11.71 (25)	0.381	0.5075/0.6538
NOT_1	2124	10.72 (25)	0.264	0.4921/0.5053
NOT_2	2136	12.20 (20)	0.293	0.5118/0.6025
$CNOT_1$ [a]	2115	NR (30)	0.592	0.6877/0.7249
$ACNOT_2$ [a]	2147	NR (20)	0.232	0.6374/0.8924

[a]Reference 15.

tude $A(\nu_j)$ and phase $\phi(\nu_j)$ components, resulting in a frequency step of $d\nu=10\ \text{cm}^{-1}$.

A result of having 51 discrete ν_j frequency components is that the spectrum contains steplike features. To our knowledge, other theoretical pulse shaping studies have not used discretized frequencies.[30–32] Rather, once the frequencies with associated amplitude and phase components (51 here) are chosen, they are cubic spline interpolated to produce a smooth spectrum. Cubic spline fitting, as seen in other studies, can result in elements of $\epsilon(\nu)$ which extend beyond the limits initially set by the TL pulse. In the present study, the frequency domain field $\epsilon(\nu)$ is Fourier transformed (integrated) as a sum of rectangles rather than via a spline fit. In the time domain, the electric field $\epsilon(t)$ is truncated at $\pm(0.5n-1)/2T$ of the central time, where n is the total number of parameters optimized $(51\times2=102)$ and T is half of the entire frequency range $(250\ \text{cm}^{-1})$. This gives a total temporal pulse duration of 6.67 ps. The integrated laser pulse energy E is given as[15]

$$\frac{E}{A}=c\varepsilon_0\int|\epsilon(\nu)|^2d\nu, \tag{8}$$

where c is the speed of light, ε_0 is the permittivity of free space, and A is the area illuminated by the laser field. In the results presented, the pulse area corresponds to a beam focused down to a diameter of 50 μm. The energy and amplitude of the frequency domain TL pulse are used as a reference to properly normalize and construct the correct time domain laser pulse intensity. Varying the total energy within the original TL pulse dictates the fraction of this energy that will be part of the resulting optimized laser pulse energy and its corresponding intensity.

In the context of this study, the simplest amplitude and phase shaped laser pulse is examined, namely, a binary pulse. This constitutes two choices for both the amplitude and phase, being 0 or 1, and 0 or π, respectively. Substitution of all four combinations of these binary amplitude and phase parameters into Eq. (7) yields unique values for $\sqrt{A(\nu_j)}\exp[i\phi(\nu_j)]=0,\pm1$. This results in a real valued three parameter choice for the total amplitude of $\epsilon(\nu)$ for each frequency value ν_j. The binary pulse shape is important since all general pulse shaping experiments optimize in a search space in which the binary pulse shape is already a solution. For example, a pulse shaper with a choice of eight amplitude and phase components will by default also contain the amplitude parameters 0 and 1, and also the phase parameters 0 and π. Thus there is the possibility that the binary pulse could be chosen as the optimal pulse shape. Studying simple binary pulse shapes sets the lower bounds for the fidelity of the quantum gate operations, while allowing for a much simpler parameter search space. In the current study the parameter search space for a binary pulse consists of 3^{51} possible combinations of amplitude and phase, while a pulse shaper with eight independent amplitude and phase components would result in a parameter search space of $(8\times8-1)^{51}=21^{51}\times3^{51}$. The search space size has an effect on the ability for the optimization algorithm to find the optimal solution efficiently and the credibility of that solution.

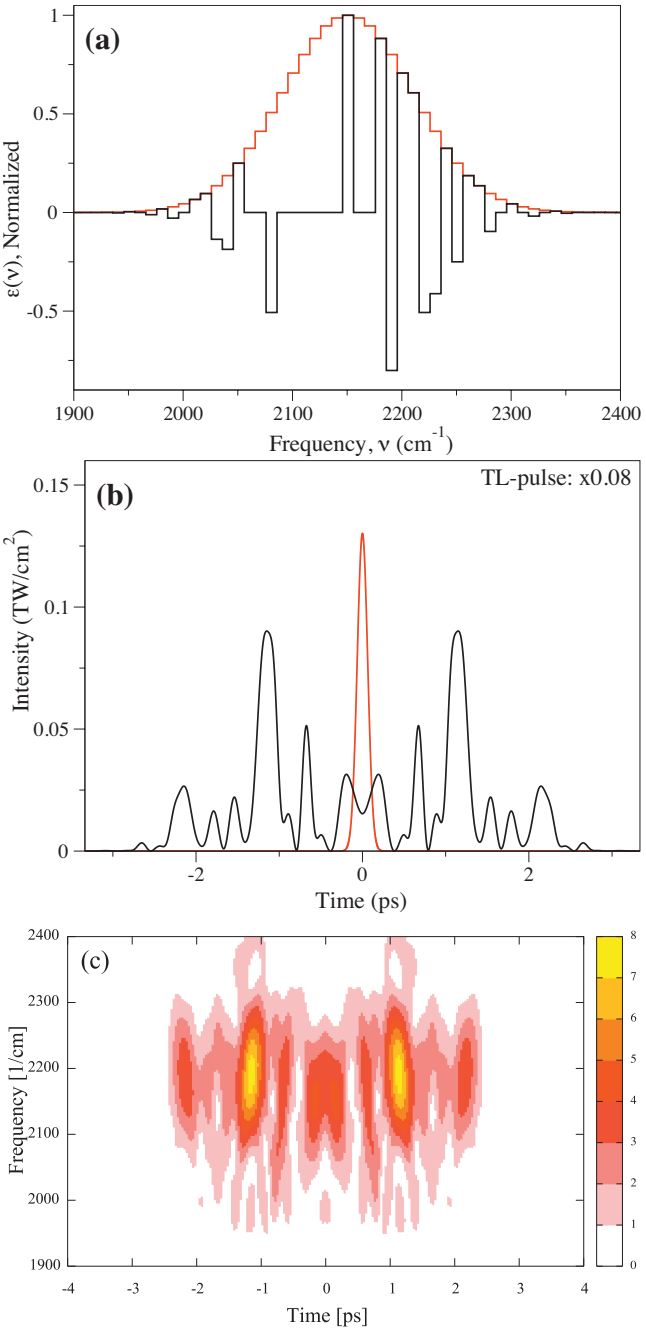

FIG. 2. Resulting laser pulse for the optimized ACNOT$_1$ quantum gate at $E_{pulse}=4.07$ μJ. (a) Frequency domain $\epsilon(\nu)$, where negative values denote a phase $\phi(\nu)=\pi$. Red: TL pulse. Black: optimized pulse. (b) Time domain intensity $|\epsilon(t)|^2$. Red: TL pulse (intensity scaled by a factor of 0.08). Black: optimized pulse. (c) cross-correlation frequency resolved optical gating (XFROG) trace for the obtained optimal field.

Binary pulse optimization has other interesting characteristics that have been explored previously. First, it will produce a laser pulse which is symmetric in the time domain. Second, binary shaped laser pulses direct the target state populations of the individual gate transitions to phase-aligned solutions. Work of Schröder and Brown[33] demonstrated the use of temporally symmetric pulses for quantum gate operations using OCT with a filter function. Laser pulses symmetric in time occurred naturally as the most efficient means of control in other studies examining NOT gates optimized with (nonfiltered) OCT.[34,35] In experimental

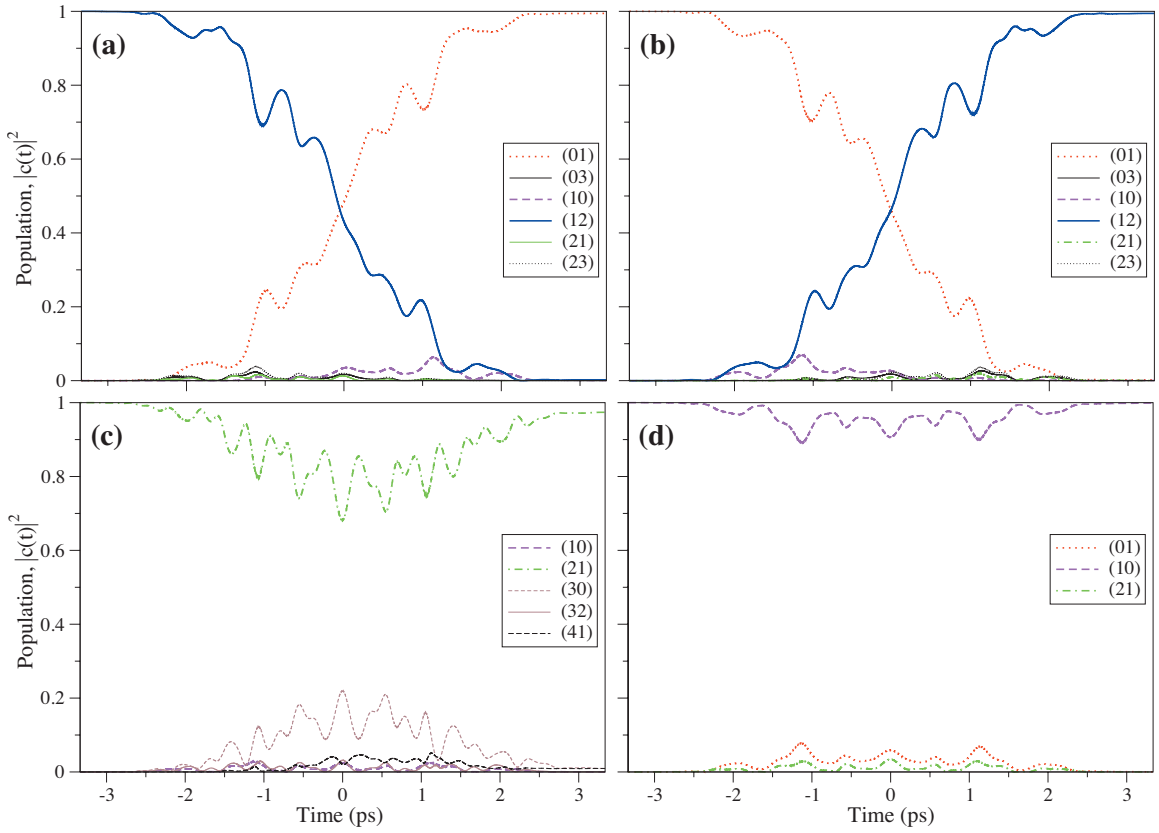

FIG. 3. Resulting populations for the optimized $ACNOT_1$ quantum gate at $E_{pulse}=4.07$ μJ. [(a)–(d)] Propagation of states with the $ACNOT_1$ optimized laser pulse over the pulse duration for transitions: (a) $|00\rangle \rightarrow |01\rangle$, (b) $|01\rangle \rightarrow |00\rangle$, (c) $|10\rangle \rightarrow |10\rangle$, and (d) $|11\rangle \rightarrow |11\rangle$. The most important contributing rovibrational states are shown.

studies of Lozovoy *et al.*,[36] molecular fragmentation was selectively controlled using only binary phase shaped laser pulses.

In order to search through the combinations of amplitude and phase which produce the optimal pulse shape for the quantum gate operation being studied, the GA optimization routine is utilized.[37] The GA uses the general ideas behind natural selection and survival of the fittest to logically determine the optimal pulse shape to cause the greatest fidelity, without having to evaluate all possible combinations of amplitude and phase. Within this particular GA, we chose to use *elitism* and the *micro-GA* procedures rather than mutation. Elitism is when the highest fidelity individual from the previous generation is automatically included in the construction of the new generation. The micro-GA eliminates biological interbreeding by restarting the generation with the *elite* individual and randomly selected individuals, when the individuals (laser pulses) of a generation become too similar. The GA is chosen to produce 500 generations with eight individuals in each. With these choices of GA parameters, a minimal change in the fidelity (less than 0.2% and usually less than 0.05%) was observed for the elite individuals between generations 400 and 500, suggesting that the calculation was near the global maximum fidelity.

III. RESULTS AND DISCUSSION

A. Optimal quantum gates

In order to determine the maximum fidelities of the quantum gates studied at the chosen central frequencies and frequency discretization, nine different total TL-pulse energies were chosen, i.e., (5, 7, 10, 15, 20, 25, 30, 35, and 60 μJ). The optimal laser pulses which produce the greatest fidelity for each quantum gate are listed in Table II, along with the associated central frequency, pulse energy, and peak intensity. The total energy contained in the TL pulse and optimized pulse was determined by Eq. (8). The central frequency ν_0 was chosen as the resonant frequency for gates involving a single transition (CNOT/ACNOT) or the average frequency if there were two resonant frequencies involved (NOT/Had). There is a distinct gap between the fidelities obtained for the CNOT and ACNOT gates, compared with the Had and NOT gates. While all the fidelities from the CNOT and ACNOT pulses are greater than or equal to 0.80, the greatest fidelity obtained from the Had and NOT pulses is 0.62 (Had_1). It also seems that the average population $\bar{P}$ for optimized laser fields for the Had and NOT gates is also around 0.60. Not only do the optimized laser fields for the Had and NOT gates have difficulty in producing a global phase, they also struggle at transferring population compared with the CNOT and ACNOT gates. As described previously, the Had and NOT quantum gates here act as 2 qubit operations and are not explicitly 1 qubit, as they are usually treated. The poor fidelities obtained for the Had and NOT gates may be due to the fact that these gates must control an extra transition compared with the CNOT and ACNOT gates (see Table I or Fig. 1).

In Table II, there is a comparison between the $CNOT_1$ and $ACNOT_2$ quantum gates studied by Tsubouchi and

Momose,[15] who also used CO as a candidate molecule. The differences between their study and this one are that they smoothed their frequency domain field $\epsilon(\nu)$ using cubic spline interpolation, chose different rovibrational states to represent the qubits, and optimized laser pulses with a choice of 64 amplitude and phase components. As previously stated, their choice of qubits resulted in quantum gate operations which included two-photon transitions. Our qubit representation is chosen such that all gate operations involve only one-photon transitions. The importance of the choice of qubit states is apparent when comparing the fidelities and even the average final state populations from Tsubouchi and Momose[15] and the current study. They obtain fidelities which are at most 0.69, while we are able to produce fidelities that are greater than 0.80. Also compared with their study, we were able to utilize pulse energies and peak intensities that are much lower. Of course, these comparisons are not entirely fair due to the different choices of qubit states but it is interesting to note that the laser fields they generated are governed by independent choice of 64 amplitude and 64 phase components, which are then cubic spline fit. We use only two amplitude and two phase discretized binary laser fields to produce much higher fidelities. In Secs. III B and III C, we discuss in more detail the dynamics for two quantum gates which when optimized produced a high fidelity ($ACNOT_1$) and low fidelity (NOT_2).

B. $ACNOT_1$ quantum gate

The $ACNOT_1$ quantum gate laser pulse produced the greatest fidelity (0.9729), see Table II. The resulting frequency and time domain laser pulses are shown in Fig. 2 and the resulting state populations during the pulse interaction in Fig. 3. Figure 2(a) shows the frequency domain optimized pulse $\epsilon(\nu)$ in black and the TL pulse in red. They are discrete and the optimized laser pulse is composed of select frequencies bound by the TL-pulse's Gaussian shape. Negative amplitudes depict phase values of π radians. The main features to notice within Fig. 2(a) are that the $ACNOT_1$ quantum gate is centered at ν_0=2151 cm^{-1} and the GA chooses this frequency, which is associated with the needed $|00\rangle \leftrightarrow |01\rangle$ transition, i.e., $(\nu J)=(01)\leftrightarrow(12)$. The frequencies the GA does not include are those associated with transitions between other qubits, namely, the $(10)\leftrightarrow(01)$, $(10)\leftrightarrow(21)$, and $(21)\leftrightarrow(12)$ transitions, i.e., 2139, 2121, and 2109 cm^{-1}, respectively. These frequency components are located within the large zero amplitude region to the left of the central frequency. The square of the Fourier transform of this frequency domain field produces the time domain laser pulse intensity profile, Fig. 2(b), when truncated to a maximum temporal width of 6.67 ps, as specified previously. Shown in this figure is the optimized laser field (black) along with the TL pulse (red) scaled down by a factor of 0.08. The TL pulse has a peak intensity of 1.63 TW/cm^2, while that of the optimized laser pulse is only 0.09 TW/cm^2. Another feature is that the TL pulse has a FWHM temporal width of Δt =147 fs, while the optimized laser pulse has stretched to ~5.5 ps. The optimized laser field also contains 4.07 μJ of the total original 10 μJ from the TL pulse.

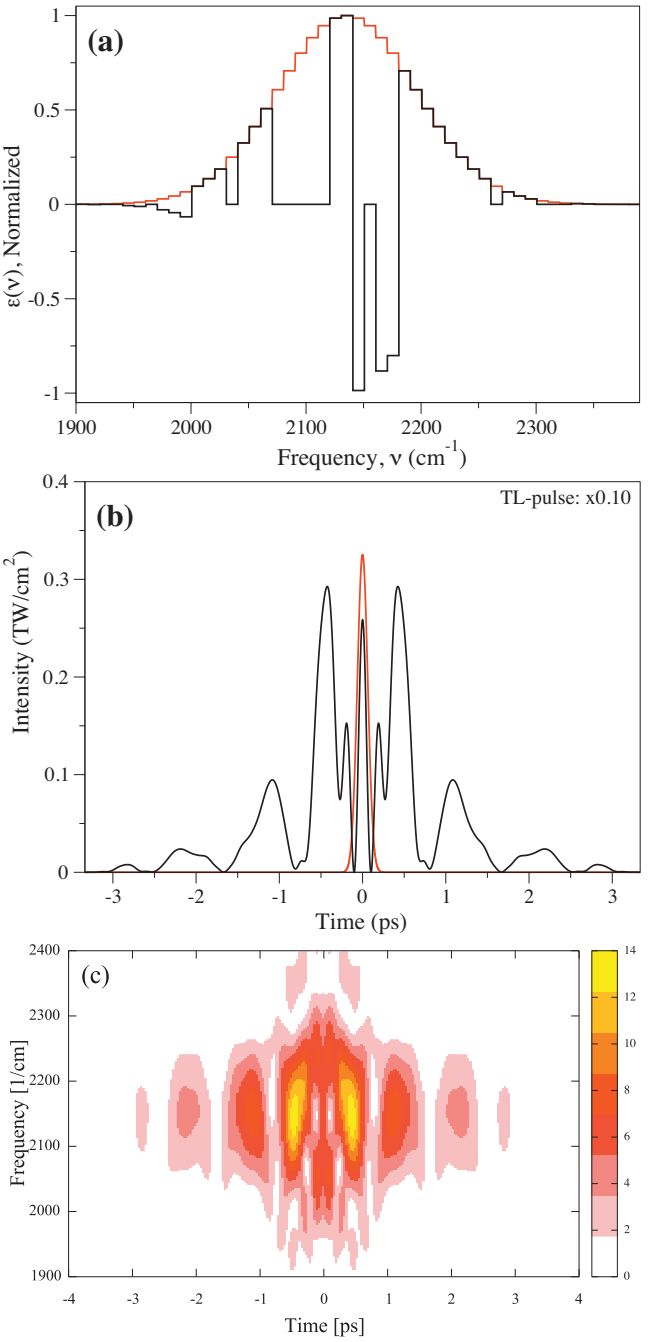

FIG. 4. Resulting laser pulse for the optimized NOT_2 quantum gate at E_{pulse}=12.20 μJ. (a) Frequency domain $\epsilon(\nu)$, where negative values denote a phase $\phi(\nu)=\pi$ radian. Red: TL pulse. Black: optimized pulse. (b) Time domain intensity $|\epsilon(t)|^2$. Red: TL pulse (intensity scaled by a factor of 0.10). Black: optimized pulse. (c) XFROG trace for the obtained optimal field.

The state transitions that the $ACNOT_1$ gate must control, see Table I, are shown in the state population graphs of Figs. 3(a)–3(d). Since the average population is relatively high at 0.9904, it is expected that all transitions are well controlled. The $|00\rangle \leftrightarrow |01\rangle$ transition according to Figs. 3(a) and 3(b) occurs via a complex two-state transfer, with little excitation of outlying states. For the other qubit states of the $ACNOT_1$ gate operation, they must remain the same after the laser field interaction. The only change that must occur is that both qubits $|10\rangle$ and $|11\rangle$ must acquire a global phase change, as did the transition $|00\rangle \leftrightarrow |01\rangle$. For this to occur the states

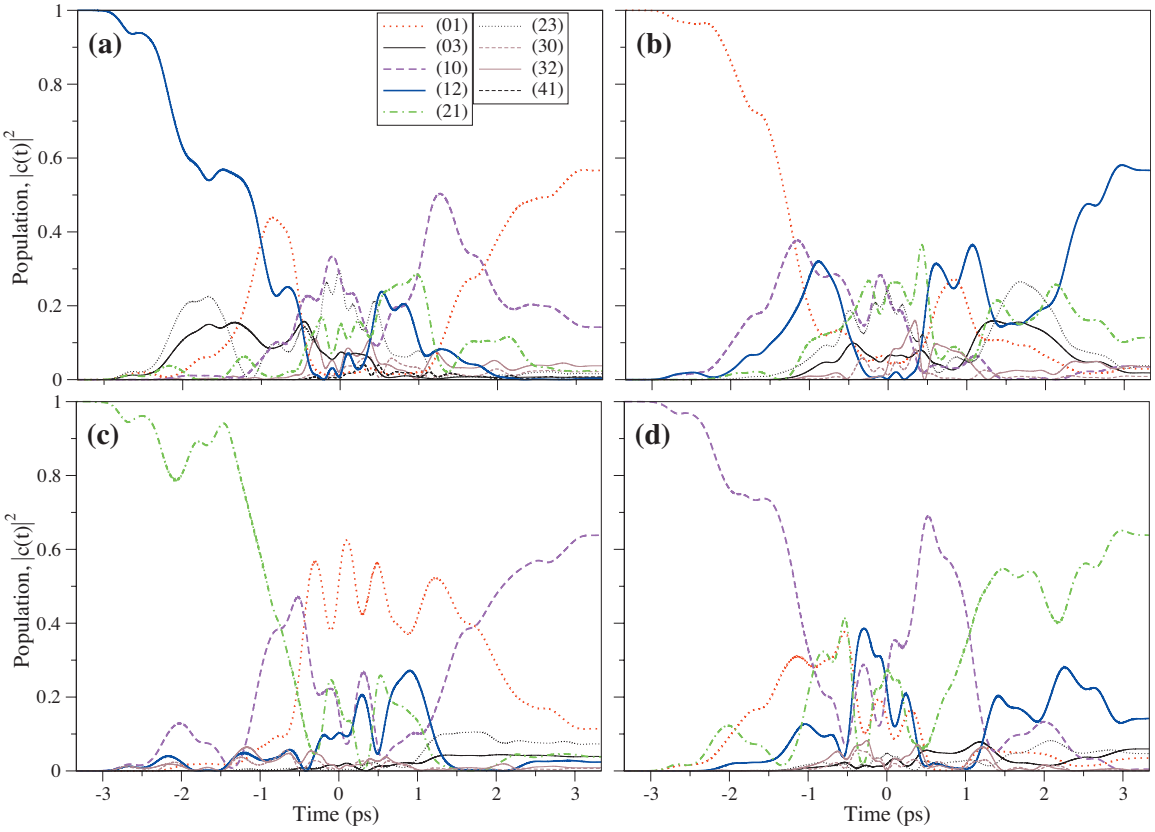

FIG. 5. Resulting populations for the optimized NOT_2 quantum gate at $E_{pulse}=12.20\ \mu J$. [(a)–(d)] Propagation of states with the NOT_2 optimized laser pulse over the pulse duration for transitions: (a) $|00\rangle \rightarrow |01\rangle$, (b) $|01\rangle \rightarrow |00\rangle$, (c) $|10\rangle \rightarrow |11\rangle$, and (d) $|11\rangle \rightarrow |10\rangle$. The most important contributing rovibrational states are shown.

must undergo some population change and this is seen in Figs. 3(c) and 3(d). The resulting phase changes undergone in the qubit transformations $|00\rangle \leftrightarrow |01\rangle$, $|10\rangle \rightarrow |10\rangle$, and $|11\rangle \rightarrow |11\rangle$ are -1.055, -1.303, and -0.937 rad, respectively. The phase change for the $|10\rangle \rightarrow |10\rangle$ transition is higher than that obtained for the other two qubit transformations. This could be due to some population being lost from the qubit state $|10\rangle$ by the end of the pulse interaction resulting in $P_{(21)}=0.9739$, compared with the final populations of the other states $P_{(12)/(01)}=0.9944$ and $P_{(10)}=0.9988$.

C. NOT_2 quantum gate

The optimal NOT_2 quantum gate laser pulse is shown in Fig. 4 in both the frequency and time domains. The resulting population transitions for the gate operation are in Fig. 5. The optimal NOT_2 gate laser pulse has frequency components associated with the gate transitions $(21) \leftrightarrow (10)$ and $(12) \leftrightarrow (01)$, 2121, and 2151 cm^{-1}, respectively, as well as 2139 cm^{-1}, which is the $(10) \leftrightarrow (01)$ transition not required for the NOT_2 gate operation. The $(21) \leftrightarrow (12)$ transition frequency 2109 cm^{-1} is not present. The resulting intensity of the laser pulse in the time domain is shown in Fig. 4(b), where the TL pulse has been scaled down by a factor of 0.10. The TL pulse this time has a peak intensity of 3.25 TW/cm^2, while the optimized laser pulse has a peak of 0.29 TW/cm^2. The TL pulse has a temporal width of $\Delta t = 147$ fs, while the optimized laser pulse spans a length of ~ 6 ps and contains 12.20 μJ of the total original 20 μJ from the TL pulse.

The average final population obtained for the optimal NOT_2 quantum gate is 0.6025, indicating that the laser pulse populates other accessible states. This is shown in Figs. 5(a)–5(d), where there are many other states appreciably populated by the end of the pulse duration. Excitation to other nonqubit states is seen for all optimal laser pulses obtained for the Had and NOT gates.

The fidelities for the Had and NOT gates are not as high as those obtained for the CNOT and ACNOT gates. The implications of this is that the qubit states under the quantum gate operation, which must acquire a global phase by the end of the pulse duration, are in fact not coherent. The phase changes undergone during the NOT_2 operation, for example, are -0.4817 and 0.3136 rad for the transitions $|10\rangle \rightarrow |11\rangle$ and $|00\rangle \rightarrow |01\rangle$, respectively. The phase changes may be of similar magnitude but are different by a shift in over $\pi/4$ rad. Indeed the NOT_2 gate and other binary laser pulses optimized for the Had and NOT quantum gates have difficulty in controlling not only the average population but also the global phase.

IV. CONCLUSION

It was shown in this study that simple binary shaped pulses can provide sufficiently good control for quantum gate operations with a proper choice of qubits represented by

rovibrational states of $^{12}C^{16}O$. In some cases, as in the CNOT and ACNOT gates, remarkable control is achieved considering the simplicity of the binary pulse shape. The fidelities obtained further improve on previous work by Tsubouchi and Momose,[15] in which they used a variation of 64 amplitudes and 64 phases, along with a qubit representation that included two-photon transitions. As a result, the optimal input pulse energies and peak intensities produced for the CNOT and ACNOT gates were much larger than those needed in our study. The optimized NOT and Had gate laser pulses produced only moderate fidelities since the required 2 qubit operation consisted of controlling population and phase between all four qubits simultaneously. Current work is directed at investigating general properties of molecular systems and pulse shapers in order to deduce crucial requirements for control of molecular states with shaped laser pulses. Future work involves studying in more detail the underlying features of binary pulses which allows them to exhibit such good control.

ACKNOWLEDGMENTS

The authors would like to thank the Alberta Ingenuity Fund (New Faculty Award) and Natural Sciences and Engineering Research Council of Canada (NSERC Discovery Grant) for financial support. We thank the Canadian Foundation for Innovation (New Opportunities Fund) for support of the computational infrastructure on which this work was carried out.

[1] M. Shapiro and P. Brumer, *Principles of the Quantum Control of Molecular Processes* (Wiley, New York, 2003).
[2] S. A. Rice and M. Zhao, *Optical Control of Molecular Dynamics* (Wiley, New York, 2000).
[3] G. G. Balint-Kurti, S. Zou, and A. Brown, Adv. Chem. Phys. **138**, 43 (2008).
[4] M. Dantus and V. Lozovoy, Chem. Rev. (Washington, D.C.) **104**, 1813 (2004).
[5] T. Brixner and G. Gerber, ChemPhysChem **4**, 418 (2003).
[6] I. Znakovskaya, P. von den Hoff, S. Zherebtsov, A. Wirth, O. Herrwerth, M. J. J. Vrakking, R. de Vivie-Riedle, and M. F. Kling, Phys. Rev. Lett. **103**, 103002 (2009).
[7] T. Zuo, A. Bandrauk, and P. Corkum, Chem. Phys. Lett. **259**, 313 (1996).
[8] G. Yudin, A. Bandrauk, and P. Corkum, Phys. Rev. Lett. **96**, 063002 (2006).
[9] C. Tesch and R. de Vivie-Riedle, Phys. Rev. Lett. **89**, 157901 (2002).
[10] D. Babikov, J. Chem. Phys. **121**, 7577 (2004).
[11] K. Shioya, K. Mishima, and K. Yamashita, Mol. Phys. **105**, 1283 (2007).
[12] C. Tesch, L. Kurtz, and R. de Vivie-Riedle, Chem. Phys. Lett. **343**, 633 (2001).
[13] B. Korff, U. Troppmann, K. Kompa, and R. de Vivie-Riedle, J. Chem. Phys. **123**, 244509 (2005).
[14] D. Weidinger and M. Gruebele, Mol. Phys. **105**, 1999 (2007).
[15] M. Tsubouchi and T. Momose, Phys. Rev. A **77**, 052326 (2008).
[16] L. Vandersypen, M. Steffen, G. Breyta, C. Yannoni, M. Sherwood, and I. L. Chuang, Nature (London) **414**, 883 (2001).
[17] E. Knill, R. Laflamme, R. Martinez, and C.-H. Tseng, Nature (London) **404**, 368 (2000).
[18] F. Schmidt-Kaler, H. Häffner, M. Riebe, S. Gulde, G. P. T. Lancaster, T. Deuschle, C. Becher, C. Roos, J. Eschner, and R. Blatt, Nature (London) **422**, 408 (2003).
[19] S. Gulde, M. Riebe, G. P. T. Lancaster, C. Becher, J. Eschner, H. Häffner, F. Schmidt-Kaler, I. L. Chuang, and R. Blatt, Nature (London) **421**, 48 (2003).
[20] J. Vala, Z. Amitay, B. Zhang, S. Leone, and R. Kosloff, Phys. Rev. A **66**, 062316 (2002).
[21] W. Zhu, J. Botina, and H. Rabitz, J. Chem. Phys. **108**, 1953 (1998).
[22] R. Judson and H. Rabitz, Phys. Rev. Lett. **68**, 1500 (1992).
[23] B. Amstrup, J. Doll, R. Sauerbrey, G. Szabo, and A. Lorincz, Phys. Rev. A **48**, 3830 (1993).
[24] C. Gollub and R. de Vivie-Riedle, Phys. Rev. A **79**, 021401 (2009).
[25] A. W. Mantz, J. P. Maillard, W. B. Roh, and K. N. Rao, J. Mol. Spectrosc. **57**, 155 (1975).
[26] D. Goorvitch and C. Chackerian, Astrophys. J., Suppl. Ser. **91**, 483 (1994).
[27] J. Ahn, T. C. Weinacht, and P. H. Bucksbaum, Science **287**, 463 (2000).
[28] J. Palao and R. Kosloff, Phys. Rev. A **68**, 062308 (2003).
[29] C. Tesch and R. de Vivie-Riedle, J. Chem. Phys. **121**, 12158 (2004).
[30] C. Gollub and R. de Vivie-Riedle, Phys. Rev. A **78**, 033424 (2008).
[31] M. Tsubouchi, A. Khramov, and T. Momose, Phys. Rev. A **77**, 023405 (2008).
[32] F. Langhojer, D. Cardoza, M. Baertschy, and T. Weinacht, J. Chem. Phys. **122**, 014102 (2005).
[33] M. Schröder and A. Brown, New J. Phys. **11**, 105031 (2009).
[34] U. Troppmann and R. de Vivie-Riedle, J. Chem. Phys. **122**, 154105 (2005).
[35] B. Schneider, C. Gollub, K. Kompa, and R. de Vivie-Riedle, Chem. Phys. **338**, 291 (2007).
[36] V. Lozovoy, T. Gunaratne, J. Shane, and M. Dantus, ChemPhysChem **7**, 2471 (2006).
[37] D. L. Carroll, v1.7a (2004), http://www.cuaerospace.com/carroll/ga.html.